Modeling of internal residual stress in linear and branched polyethylene films during cast film extrusion: Towards a prediction of heat-shrinkability

Violette Bourg, P. Ienny, A. S. Caro-Bretelle, N. Le Moigne, Valérie Guillard, A. Bergeret

Modeling of internal residual stress in linear and branched polyethylene films during cast film extrusion: Towards a prediction of heat-shrinkability

V. Bourg[a,b,c], P. Ienny[a,*], A.S. Caro-Bretelle[a], N. Le Moigne[a], V. Guillard[b], A. Bergeret[a]

[a] C2MA, IMT Mines Ales, Université de Montpellier, 6 avenue de Clavières, 30100 Alès, France
[b] Ingénierie des Agropolymères et Technologies Emergentes-UMR 1208 IATE, Université Montpellier 2, CC023 Pl. E. Bataillon, F-34095, Montpellier, France
[c] CREPEC, Research Center for High Performance Polymer and Composite Systems, Department of Chemical Engineering, Polytechnique Montreal, C.P. 6079, Montreal, QC, H3C 3A7, Canada

A B S T R A C T

The singular property of shrinkage is used in the packaging sector to wrap products. Polyethylene film products are mostly produced by either blown or cast film extrusion. During processing, under the effect of drawing, the molten polymer is stretched in one or two dimensions according to the cast or blown film extrusion. When the resulting solid film is subjected to a sudden increase in temperature, it shrinks as a result of the relaxation of polymer chains that were oriented under stress and frozen in a stretched state upon processing resulting in internal residual stresses. A general viscoelastic model in the framework of large strain has been used to predict the development of the internal residual stresses stored during the stretching stage of the process. Linear and branched polyethylenes (LLDPE, LDPE) were used as model matrices and additional blends (80/20%, 50/50%and 20/80% LDPE/LLDPE w/w) of pure resins were also studied. Moreover, as properties of stretched films are highly dependent on processing conditions, the influence of the draw ratio was also investigated. Contrasted mechanical response in strain of the LDPE and LLDPE films under stretching were observed and justified by differences in their rheological behavior due to long branch chains (LCB) in LDPE. The modeled ultimate stress stored in LDPE and LLDPE films was compared to the shrinkage stress measured by Dynamic Mechanical and Thermal Analysis (DMTA). Both stresses were found to be in the same order of magnitude which constitutes an interesting result for the prediction of heat-skrinkability of stretched polymer films.

Keywords:
Polyethylene
Modeling
Cast film extrusion
Shrinkage
Internal residual stress

1. Introduction

Production of thin films are mostly achieved by blown or cast film extrusion and used in a large scale of applications such as packaging (McNally, 2005). One important property of these thin films is their heat-shrinkability used to gather products. The shrinkage property is a direct consequence of the stretching of a molten polymer followed by a rapid quenching to freeze both the stress and the deformation undergone during the process (Haudin et al., 2003). Indeed, Haudin et al. (2003) showed that the shrinkage is the direct consequence of the fusion of the crystallites leading to an oriented amorphous phase in which the extended chains tend to recoil isotopically when reheated above its melting temperature.

The shrinkage property is therefore divided in two principal characteristics namely, the shrinkage rate and the shrinkage stress required so that the polymer film shrinks tight around the product and fulfill its function.

In the cast film extrusion process, the molten polymer is extruded flat through a slit die and then stretched in the air while a reduction in both its thickness and width occurs. During the stretching in the path between the extruder die and the rolls, the film is subjected both to a large extension in the longitudinal direction and to a continuous cooling flow. Finally, the molten polymer is quenched on thermo-regulated rolls of the haul-off unit. When the film reaches the rolls, the temperature sudden drop leads to the crystallization resulting in the change from molten to solid state, preventing from any further decrease in width and thickness of the film. The deformation and the cooling conditions that take place in the air gap and onto the rolls directly affect the final properties of the film (such as optical properties, mechanical characteristics …) (Barot and Rao, 2005).

Thus, the modeling of the cast film extrusion process can be divided in two stages: the first stage can be modeled considering the thermo-mechanical behavior of the molten polymer during the path of stretching in air (sometimes referred by authors as primary film (Barq

* Corresponding author.
E-mail address: patrick.ienny@mines-ales.fr (P. Ienny).

et al., 1992)) and the second stage that can be modeled using a purely thermal model of the polymer crystallization occurring onto the rolls (Jay et al., 1998).

The first mathematical and physical description of the cast film process was introduced by Pearson in 1966 (Pearson, 1966) and then by Sergent in 1977 (Sergent, 1977). These authors considered the process as isothermal (*i.e.,* it did not take into account the polymer solidification) and the stretching was assumed as being unidimensional. Moreover, the molten polymer was considered as a Newtonian fluid. Later, Cotto et al. (Cotto et al., 1989) used a thermomechanical model for the overall process that took into account the polymer crystallization to relate the influence of the temperature of the rolls on the formation of crystalline structures and morphologies. This thermomechanical behavior was used to build a process modeling based on the growing of the internal residual stress into the primary film, and a purely thermal model reflecting the crystallization related to the cooling on the roll was used for the second stage of the process. In their model, Cotto et al. used an approximation of the stress by using a simplified isothermal Newtonian model and by assuming a constant width even though they experimentally observed a slight contraction of the film during stretching in air. In addition, the model considered a mean elongation rate and a variation of viscosity with temperature described by an Arrhenius law. According to this modeling, the evaluated residual stress stored in the polymer film (homopolymer isotactic polypropylene PP) ranged between 4.45 x10^3 Pa and 1.762 x 10^4 Pa. The objective of this study was to correlate the microstructure of a series of PP films with their processing conditions. Indeed, it was already well-known that for an increasing flow intensity, the following morphologies are likely to be observed: spherulites, ellipsoidal spherulites, sheaf-like and finally cylindrites (as proposed in Keller's row-nucleated morphology model (Keller and Machin, 1967)). Here, they found that the morphological features were not affected by the narrow range of stresses tested.

More recently, Barot and Rao (Barot and Rao, 2005) used a combination of a generalized Maxwell model considering the melt as viscoelastic and a non-Hookean model to describe the transition of the molten polymer from a viscoelastic fluid to an elastic solid. However, they found out that the initial thickness taken into account as a boundary condition was over-estimated probably due to the fact that they neglected the "die-swell effect" and also because they used a single element of Maxwell. Even though the viscoelastic behavior would have required multiple relaxation mechanisms to be modeled adequately.

Even if a lot of efforts have been made in the modeling of the polymer film casting process over these past 30 years, only a few papers reported experimental data for model validation. In the present study, it is proposed an innovative modeling method to predict the shrinkage stress from the internal residual stress stored by the polymer film during the cast film extrusion process.

During processing, the molten polymer behaves as a non-Newtonian incompressible viscoelastic fluid and then undergoes large deformations and rapid cooling onto the thermostated rolls, resulting in a semi-crystalline solid film. Thereby, all the deformations take place before the material touches the rolls where the film undergoes a rapid quenching. On this basis, the tailor-made procedure of the modeling of internal residual stress and comparison with shrinkage stress was conducted as follows:

- First, the rheological model parameters were identified from rheological experiments under oscillatory shear small deformation at different temperatures,
- Then, during the process, thermal and bidimensional kinematic boundary conditions were evaluated through optical instrumentation,
- Finally, the implementation of the rheological behavior in the numerical modeling of the process associated with the boundary conditions leads to an estimation of the internal residual stress stored in plane directions while stretching,
- The resulting modeled internal residual stress was then correlated to the restraint shrinkage stress determined by DMTA tests. Results obtained from various polyethylenes with different macromolecular structures (linear, branched) and their blends were finally discussed.

This study is thus devoted to the experimental and modeling of the cast film process and the understanding of the thermo-mechanical history of the material from the molten state to the heat-shrinkability of the casted films.

Shrinkage stress measurements thanks DMTA have been investigated for sake of comparison with the modeled internal residual stress. In the discussion part, insights are proposed to explain the deviation from the model.

2. Materials

A Low-Density Poly(Ethylene) (LDPE) film grade produced by ExxonMobil 171BA® and a Linear Low-Density Polyethylene with butene comonomer (LLDPE) film grade produced by Polimeri Europa commercialized under the trade name Flexirene FG30® were used as model matrices. LDPE is produced by high pressure/high temperature autoclave polymerization favorable to create long-chain branched (LCB) macromolecules with some short-chain branched (SCB) macromolecules on the sides of the polymer backbone (Ward, 1997). On the other hand, linear PE is produced by the copolymerization of ethylene and butene which leads to the formation of short chain branches of 4 carbon length (*i.e.,* ethyl). The main properties of the LDPE and LLDPE matrices given in the supplier datasheets are presented in Table 1.

Three additional blends consisting in various amounts of LDPE/LLDPE (20/80%, 50/50% and 80/20% LDPE/LLDPE w/w) were studied. Pellets of LLDPE and LDPE were directly dried mixed and melt-compounded in the extruder.

3. LDPE, LLDPE and their blends processing

Cast film extrusion was performed with a laboratory-scale extruder Polylab system composed of a HAAKE RheoDrive4 motor unit/torque rheometer with three thermoregulated zones coupled with a HAAKE Rheomex 19/25 OS single screw extruder (with a Maddock screw). The extruder temperature barrel was fixed between 210 and 220 °C and the die at 230 °C. The screw speed was kept constant at 100 rpm. The extruder unit was equipped with a fish-tail designed die to process the molten polymer into a film. The die width was $l_0 = 270$ mm and the die gap was set at $e_0 = 0.45$ mm. The system was piloted by PolySoft OS® software to set and control temperature zones, screw speed and torque (internal pressure). The extruder was connected to the air network which provides ambient temperature air to cool the hopper zone. The stretching of the molten polymer was carried out with a floor standing two-roll haul-off Thermo SCIENTIFIC unit with line speed ranged between $v_x =$ [1– 11] m/min, cooled at 7 °C by rustproof liquid with a HAAKE Phoenix II P1 thermostat (Thermo SCIENTIFIC) equipped with a regulated speed pump.

A stretching distance of $X = 135$ mm was chosen, so that the polymer crystallization occurs only when being quenched onto the rolls (*i.e.,* there is no more deformation as soon as the film touch the rolls (Jay et al., 1998)).

Table 1
Density (ρ), [1] Melt Flow Rate (under a load of 216 kg at 190 °C), melting temperature (T_m) and structure of LDPE and LLDPE as given in supplier datasheets.

	ρ (g. cm^{-3})	[1]MFR (g.10 min^{-1})	T_m (°C)	Structure
LDPE	0.929	0.55	114	LCB/SCB
LLDPE	0.925	1	124	SCB

Table 2
Processing parameters of LDPE, LLDPE and their blends: $\dot{m}$ mass flow rate; v_0 velocity of the melt at the die exit.

LDPE/LLDPE (%)	$\dot{m}$ (kg. h^{-1})	v_0 (mm.s^{-1})
100/0	3.5	9.09
80/20	3.3	8.58
50/50	3.2	8.39
20/80	3.3	8.62
0/100	3.2	8.27

Lamberti et al. (Lamberti et al., 2002) have proposed to increase the distance from the die to the roll (take-up distance) usually used for industrial purpose in order to compel the crystallization to occur during the path in air. This would require taking account for the crystallization when modeling the width of the film during the stretching. Although our model does not consider the crystallization, the reduced distance between the die and the chill roll leads to consider a biaxial solicitation: depending on the draw ratio, the temperature and the material architecture, this solicitation will extend from uniaxial tensile one to pure shear one. This aspect requires having a method for measuring the biaxial deformations in the plane of the film.

The velocity of the melt at the die exit v_0 is given by Eq. (1).

$$v_0 = \frac{\dot{m}}{\rho_T S_0} \tag{1}$$

where $\dot{m}$ is the mass flow rate, ρ_T is the melt density and S_0 is the cross section of the die.

The mass flow rate was evaluated by weighing the melt extrudate during 2 min (in triplicate for checking reproducibility). An approximation was made on the melt density ρ_T by using the density at ambient temperature ρ reported in Table 1. Table 2 summarizes the mass flow rate $\dot{m}$ and velocity of the melt at the die exit v_0 for the different materials used in this study.

The take-up speed v_x was measured thanks to a contact velocimeter. The take-up velocity of the rolls was used to control the draw ratio DR given in Eq. (2) and all the processing variables were kept constant for all tests (temperature, screw speed and distance). The biaxial deformation leads to define also a contraction ratio CR given in Eq. 3) where l_x is the final width of the solid film, and l_0 is the width of the die.

$$DR = \frac{v_x}{v_0} \tag{2}$$

$$CR = \frac{l_x}{l_0} \tag{3}$$

Every formulation was processed under the same operating conditions and stretched at increasing rates which are $v_1 = 61.4$ mm/s to $v_6 = 170.9$ mm/s. Furthermore, for sake of simplicity, the logarithm of DR and CR denoted E_{L_M} ("M" for machine) and E_{L_T} ("T" for transverse) were respectively used for representation. All relevant parameters are listed in Table 3.

The DR being dependent on the velocity of the melt, which is itself dependent on the density of the material, justifies the difference in kinematic ranges tested for each blend and therefore the convenience of using the notation v_1 to v_6 for take-up speeds.

The width of the solid films after chill rolls cooling exhibits different behaviors depending both on the stretching rates and the film composition (Fig. 1a). It can be observed that whatever the take-up velocity the film width is greater for LDPE and LDPE/LLDPE blends containing more than 50% LDPE. Final width (given by the contraction ratio) of LDPE-rich blends remains insensitive to the draw ratio up to the take-up speed v_4 and then slightly increases for higher draw ratios. Conversely, LLDPE width decreases continuously from low to high draw ratios. These results suggest that all films containing LCB experience a different plane strain according to the draw ratio value compared to

Table 3
Take-up speed and corresponding final dimensions of LDPE, LLDPE and LDPE/LLDPE blends: DR: draw ratio; CR: contraction ratio; E_{L_M} : log (DR); E_{L_T}: log (CR).

LDPE/LLDPE (%)	Denomination	Velocity (mm/s)	DR	CR	E_{L_M}	E_{L_T}
100/0	v_1	61.4	7.0	0.65	1.95	−0.43
	v_2	85.5	9.4	0.64	2.24	−0.44
	v_3	106.8	11.8	0.66	2.46	−0.42
	v_4	128.2	14.1	0.66	2.65	−0.41
	v_5	149.6	16.5	0.67	2.80	−0.40
	v_6	170.9	18.9	0.68	2.93	−0.38
80/20	v_1	61.4	7.5	0.66	2.01	−0.42
	v_2	85.5	10.0	0.66	2.30	−0.42
	v_3	106.8	12.5	0.66	2.52	−0.42
	v_4	128.2	14.9	0.67	2.70	−0.40
	v_5	149.6	17.4	0.68	2.86	−0.39
	v_6	170.9	19.9	0.68	2.99	−0.38
50/50	v_1	61.4	7.6	0.60	2.03	−0.51
	v_2	85.5	10.2	0.60	2.32	−0.51
	v_3	106.8	12.7	0.61	2.54	−0.50
	v_4	128.2	15.3	0.62	2.73	−0.48
	v_5	149.6	17.9	0.62	2.88	−0.47
	v_6	170.9	20.4	0.63	3.01	−0.46
20/80	v_1	61.4	7.4	0.47	2.01	−0.75
	v_2	85.5	9.9	0.46	2.29	−0.78
	v_3	106.8	12.4	0.46	2.52	−0.78
	v_4	128.2	14.9	0.45	2.70	−0.79
	v_5	149.6	17.3	0.47	2.85	−0.76
	v_6	170.9	19.8	0.47	2.99	−0.75
0/100	v_1	61.4	7.8	0.42	2.05	−0.87
	v_2	85.5	10.3	0.38	2.34	−0.97
	v_3	106.8	12.9	0.34	2.56	−1.08
	v_4	128.2	15.5	0.32	2.74	−1.14
	v_5	149.6	18.1	0.30	2.90	−1.20
	v_6	170.9	20.7	0.29	3.03	−1.24

LLDPE film that exhibit a linear chain structure. It can be assumed that adding LCB in blends prevents the film from reducing its width for the same fixed processing parameter. It highlights the importance of well characterizing the in-plane strain profile used as boundary conditions in the process modeling.

E_{L_M} as a function of E_{L_T} is plotted in Fig. 1b. As a matter of fact, these results highlight that even when processed under similar processing conditions, in which the longitudinal displacements are imposed, and transversal are undergone, the material mechanical response in strain fluctuates. These results suggest the necessity to characterize the rheological behavior in the molten state to explain the strain path undergone by the material during the stretching and its dependence on the material formulation.

4. Experimental methods

4.1. Rheological measurements

The dynamical rheological measurements of LLDPE, LDPE and their blends were performed using a strain-controlled rheometer ARES (TA Instrument) equipped with a 25 mm parallel-plate geometry in oscillatory shear mode. Prior experiments consisted in strain sweep tests at 100 rad/s for each testing temperature to determine the linear viscoelastic domain. The strain value used for all oscillatory experiments was $\gamma = 5\%$. Frequency sweep at strain $\gamma = 5\%$ were performed within the frequency ω range from 100 to 0.01 rad/s. Sample preparation consisted in the superposition of films to obtain an approximate thickness of the molten polymer of 0.8 mm after adjusting the gap between the two plates.

All measurements were reproduced twice and were well reproducible. Time sweep were conducted at $\gamma = 1\%$ and 5%, and $\omega = 1$ rad/s to check that no thermal degradation occurred during the

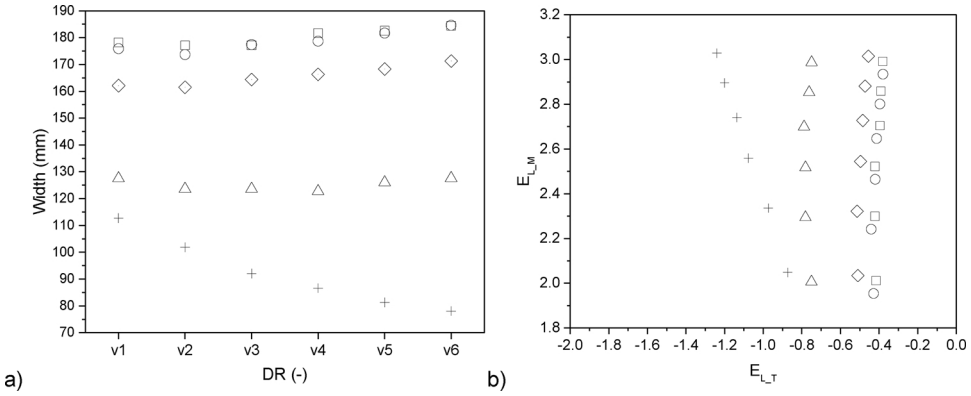

Fig. 1. (a) Width of LDPE (○), LLDPE (+) and LDPE/LLDPE blends (□) 80/20%, (◇) 50/50%, (△) 20/80% and b) Global analysis as a function of the take-up velocity v_x.

frequency sweep test. The viscoelastic parameters, namely, dynamic viscosity (η), storage modulus (G'), loss modulus (G''), complex viscosity (η^*) and loss angle (δ) (Ferry, 1980) were recorded by using TA Orchestrator® (TA Instrument) software.

The testing temperatures (150 °C, 170 °C and 190 °C) were chosen so that the polymer was above its melting temperature (to avoid any crystallization effects) and below a temperature where the material might undergo instabilities or degradation due to *e.g.*, thermo-oxidation. These conditions constitute real experimental limitations for one who attempts to model the material behavior that undergone a larger range of temperature in the process.

In this work, the isochoric viscoelastic behavior is modeled through a hereditary integral: the Piola-Kirchhoff stress tensor at a time t, $\boldsymbol{S}(t)$, is related to the deviatoric part of the Green-Lagrange strain tensor $\boldsymbol{E}(t)$ by the following equation (Green and Rivlin, 1957):

$$\boldsymbol{S}(t) = \int_0^t 2G(t-\lambda) dev(\dot{\boldsymbol{E}}(\lambda)) d\lambda \tag{4}$$

where G is the relaxation function which can be expressed in the form of Prony series:

$$G(t) = G_\infty - (G_\infty - G_0)\psi_1(t),\ \psi_1(t) = \sum_{k=1}^{N} w_k e^{\frac{-t}{\lambda_k}} \text{ with} \sum_{k=1}^{N} w_k = 1 \tag{5}$$

G_∞ and G_0 are the shear modulus, G_∞ is equal to zero at infinitely long time for molten polymers and λ_k are discrete relaxation times. This latest formulation is so-called the Generalized Maxwell Model (GMM (Laraba-Abbes et al., 2003a, 2003b)).

In the case of oscillatory shear tests at w frequency, the shear component of $\boldsymbol{E}(t)$ is $E(t) = \gamma e^{iwt}$ and the shear component of $\boldsymbol{S}(t)$ from Eq. (4) is:

$$S(t) = \left[2G_\infty - 2(G_\infty - G_0) w \sum_{k=1}^{N} \frac{w_k i\lambda_k}{iw\lambda_k + 1} \right] E(t) \tag{6}$$

The storage and loss modulus can be therefore written as:

$$G'(t) = \left[2G_\infty - 2(G_\infty - G_0) \sum_{k=1}^{N} w_k \frac{\omega^2 {\lambda_k}^2}{\omega^2 {\lambda_k}^2 + 1} \right] \tag{7}$$

$$G''(t) = \left[-2(G_\infty - G_0) \sum_{k=1}^{N} w_k \frac{\omega\lambda_k}{\omega^2 {\lambda_k}^2 + 1} \right] \tag{8}$$

4.2. Optical methods

4.2.1. Photomechanical analysis by digital image correlation

To model the internal residual stress developed during the stretching of the films, boundary conditions of strain and temperature profiles should be determined as accurately as possible from the die exit just after the die-swell region to the roll generator ($X = 135$ mm). To take into account every single phenomenon occurring during the cast film process, the die-swell region (*i.e.*, where the polymer swells at the die exit due to normal stresses in the melt) has to be considered.

To achieve this determination, a photomechanical analysis coupled with digital image correlation and infrared thermography were used. These methods allow to depict both temperature and strain profiles from the die ($X = 0$) where the material has not been stretched yet (where the temperature is roughly the one of the polymer melt in the die of the extruder) to the chill roll. To avoid the well-known "dog bone" defect (also known as "edge beads defect", *i.e.*, thickening of the films at boarders) already reported by many researchers (Agassant et al., 2005; Demay and Agassant, 1996; Lamberti et al., 2002), digital image correlation and infrared thermography has been exclusively carried out in the central zone of the films.

The boundary conditions also require the knowledge of the strain at the roll generator. This was achieved by means of both an interpolation to obtain smooth strain profile and an extrapolation to determine the boundary conditions of strain and temperature on the roll ($X = 135$ mm).

4.2.2. Digital image correlation

Image correlation or "map-matching" techniques are part of optical methods used to measure the displacement fields on a surface sample by comparing pictures acquired at different states of strain (Caro-Bretelle et al., 2013; Laraba-Abbes et al., 2003b, 2003a). This technique has been used to monitor the displacement and strain in drastic conditions such as the ones encountered at the surface of a molten polymer during processing (Boulahia et al., 2013; Muniandy et al., 2018).

A high-resolution charge-coupled device camera (Redlake Megaplus II, 1920 × 1080 continuous and square pixels, coded in 256 grey levels) was fixed to a linear stage and positioned so that the whole stretching zone of interest was recorded. The magnification was fixed up to 260 µm/pixel to keep the camera static and avoid distortion (out-of-plane) effects caused by the film thinning during the stretching. Images were recorded at a frequency of 10 Hz. The optical axis of the camera remained perpendicular to the in-plane surface of the specimen during the test. The two-dimensional coordinate system of the image corresponds to the stretching machine direction (MD) and transverse direction (TD) (Fig. 2). This coordinate system can be considered as a principal referential. From this point of view, the shear plane strain is not evaluated in the sense that it can be considered null. To improve the contrast between the translucent molten polymer and ambient white light source, a carbon black powder was used as an optical signature. The acquisition was launched when a stationary state was reached.

The digital image correlation, carried out after the test, is based on direct image correlation computation, leading to subpixel accuracy on the two-dimensional displacements components. Digital image correlation was performed with an in-house developed software, CinEMA® (Caro-Bretelle et al., 2013; Laraba-Abbes et al., 2003b, 2003a). As a matter of fact, a sequence of pictures is chosen so that (i) the first image shows the signature the closest as possible to the die and (ii) the last

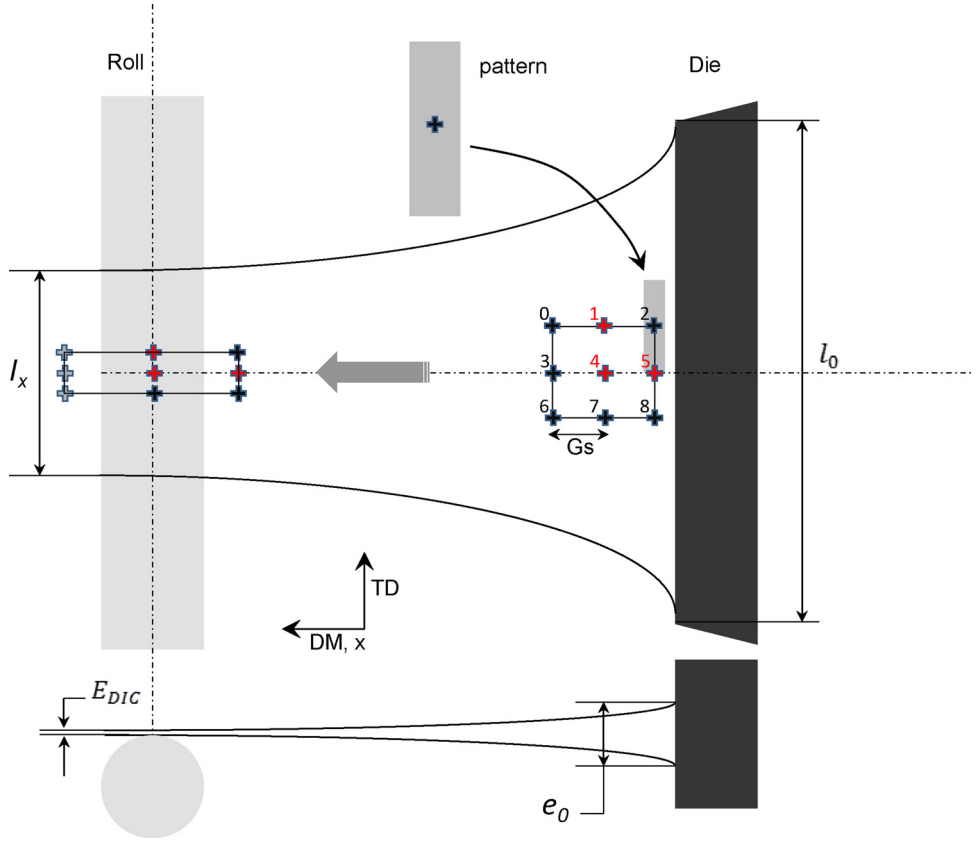

Fig. 2. Cast film extrusion: schematic principle of digital image correlation.

image shows the signature the closest as possible to the frozen line, *i.e.*, at the rolls generator, where the material strain does no longer change (Fig. 2). A virtual square mesh of 5.2 by 5.2 mm^2 on the sample is used to achieve digital image correlation in the center of the die where the stretching is supposed to be as homogeneous as possible.

From two treated images, a correlation calculation is made at every meshing point. Distance between two adjacent mesh points denoted Gs for Grid Step corresponds to the gauge lengths. Thus, stretching ratios have been measured using relative displacements between points: as shown on the Fig. 2. points 4 and 5 are used to evaluate the longitudinal stretching in the machine direction (e_{L_M}) and points 1 and 4 are used for transverse one (e_{L_T}). This new notation of the deformation is used to differentiate E_{L_M} and E_{L_T} determined by the so-called global analysis from those determined locally by photomechanical analysis. The choice of the Grid step length is a compromise between two constraints: firstly it has to be large enough to increase sensitivity for strains and secondly small enough to represent accurately the strain state as close as possible to the die.

Assuming the extra diagonal terms of the logarithmic strain tensor are equal to zero (stretching direction and x coordinate both coincide with the MD), it leads to the in-plane logarithmic strain tensor components:

$$|e_{L\_M}|_t = Ln\left(\frac{x_4(t) - x_5(t)}{x_4(t_0) - x_5(t_0)}\right) = Ln(\lambda_x(t)) \tag{9}$$

$$|e_{L\_T}|_t = Ln\left(\frac{y_1(t) - y_4(t)}{y_1(t_0) - y_4(t_0)}\right) = Ln(\lambda_y(t)) \tag{10}$$

Where $(x_i(t), y_i(t))$ correspond to the coordinates of the point "i" of the mesh at the time "t" and $\lambda_x(t)$, $\lambda_y(t)$ are the in-plane components of the strain gradient $\boldsymbol{F}$, namely principal elongations.

In addition to the previously mentioned global analysis, the photomechanical analysis allows depicting the strain path over time during the stretching and has been exclusively carried out in the central zone of the films where the deformations are more homogeneous.

However, regarding the high take-up speed tested (from v_1 = 61.4 mm/s to v_6 = 171 mm/s), the digital image correlation procedure was not able to give a satisfactory correlation rate over the entire stretching distance due to excessive deformation increment between two successive images next to the chill roll. Moreover, the prediction of the internal residual stress implies knowing the boundary conditions in terms of temperature and strain from the starting to the end of the stretching stage. Thus, it was required to interpolate the curves describing the evolution of in-plane logarithmic strain components with distance from the die (given by "X" coordinate of the point 4 – see Fig. 2). Then, the values of these components at the roll point (X = 135 mm) were extrapolated. Longitudinal and transversal interpolation/extrapolation as a function of the die distance (at X = 135 mm) according to the experimental data are shown in Fig. 3a and b, respectively in the case of LDPE.

The e_{L_M} and e_{L_T} strain profiles at low take-up speed (v_1) were found to be well fitted by the three parameters of the following equation Eq. (11). Assuming that the strain evolution with the distance from the die is similar at higher velocity, the e_{L_M} and e_{L_T} data from v_1 to $v_6$were thus also fitted with Eq. (11).

$$y = A(1 - e^{(B-CX)}) \tag{11}$$

where A, B and C are the three variable parameters, y being replaced by either e_{L_M} or e_{L_T} Then, this equation was used to extrapolate the strain from the last distance correlated to the frozen line at X = 135 mm (where the strain no longer changes).

4.2.3. *Temperature profile*

Infrared thermography was performed to determine the temperature profile along the machine direction using an infrared pyrometer Optris® PI 160 120 Hz with 160 × 120 pixels resolution detector and PI

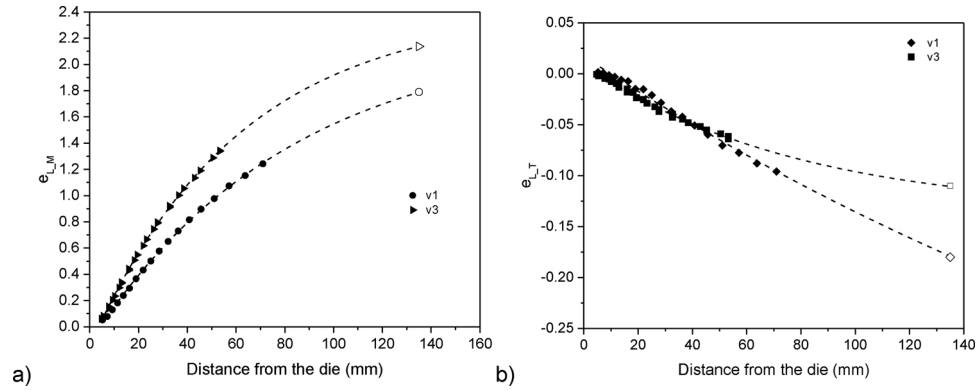

Fig. 3. Calculate strain distribution along center axis (a) MD (b) TD *versus* the distance from the die for LDPE at $v_1$and v_3. Full and open symbols represent experimental and interpolated/ extrapolated (at X = 135 mm) data respectively.

connect software. The spectral range of the infrared camera is comprised between 7.5 and 13 μm. The pyrometer was set at 50 cm above the molten polymer film to avoid contact and so that the entire stretching area could be measured. This distance is also the standard distance suggested by the camera supplier. The resolution of the area was 1.25 mm/pixel.

4.3. DMTA measurements

Restrained shrinkage tests were performed using a Dynamic Mechanical and Thermal Analysis DMTA 50 01dB-Metravib with a 0.01 N sensitivity transducer. DMTA was used upside down so that the moving part of the frame could be immersed in a thermo-regulated oil bath. Film samples of 35 mm length and 10 mm width were precisely cut along the machine direction and clamped at a fixed gauge length of 23 mm. Moreover, because of the aforementioned inhomogeneous deformations along the transverse direction, the choice of this zone is considered to be more representative of the final film properties, especially the shrinkage, which was carried out on the same representative area.

The sample was mounted between the two clamps, held taut, allowing a slight static pretension by means of the moving clamp. The restrained shrinkage test consists to measure the force released when immersing the sample into an oil bath maintained at 130 °C. During the test, the distance between clamps was maintained constant in order to avoid the sample to shrink longitudinally (restrained shrinkage). The resulting shrinkage stress was determined at the maximum force peak as the ratio between the growing force and the thickness of the initial section of the sample. The recording of the force was launched when the frame was lowered manually into the bath. Each test was reproduced at least 5 times per blend.

5. Numerical modeling

The model presented in Eqs. (4) and (5) has been implemented in its differential form through the use of internal variables. Eqs. (4) and (5) are equivalent to:

$$\begin{aligned}\boldsymbol{S}(t) &= 2G_\infty dev(\boldsymbol{E}(t)) + \sum_{k=1}^{N} -2(G_\infty - G_0)\lambda_k(dev(\boldsymbol{E}(t)) - \boldsymbol{\alpha_k}(t)) \\ &= 2G_\infty dev(\boldsymbol{E}(t)) + \sum_{k=1}^{N} \boldsymbol{X_k}(t)\end{aligned} \tag{12}$$

with

$$\lambda_k \dot{\boldsymbol{\alpha}}_k(t) = dev(\boldsymbol{E}(t)) - \boldsymbol{\alpha_k}(t),\ 1 \le k \le N \tag{13}$$

The parameters G_∞, $G_0 = \sum G_k$, λ_k, $1 \le k \le N$, are known from Table 4.

In the case of biaxial solicitation, the strain tensor $\boldsymbol{E}$, the stress tensor $\boldsymbol{S}$ and the internal variables $\boldsymbol{\alpha_k}$, $1 \le k \le N$ can be written in a tensorial form:

$$\boldsymbol{E} = \begin{pmatrix} E_x & 0 & 0 \\ 0 & E_y & 0 \\ 0 & 0 & E_z \end{pmatrix},\ \boldsymbol{S} = \begin{pmatrix} S_x & 0 & 0 \\ 0 & S_y & 0 \\ 0 & 0 & S_z \end{pmatrix},\ \boldsymbol{\alpha_k} = \begin{pmatrix} \alpha_{kx} & 0 & 0 \\ 0 & \alpha_{ky} & 0 \\ 0 & 0 & \alpha_{kz} \end{pmatrix} \tag{14}$$

Expressions of $S_x(t)$ and $S_y(t)$ are used to model the cast film extrusion process and predict the internal residual stress stored within the film during the stretching stage.

The photomechanical analysis leads to discrete variables. If the test is discretized in term of time $t_0 = [0,\ t_1,\ t_2 \ldots t_n]$ then the experimental conditions allow to access to each variable $E_x(t_p)$, $E_y(t_p)$, $p = 0 \ldots n$. $E_z(t_p)$ can be written as a function of $E_x(t_p)$, $E_y(t_p)$ and $\alpha_z(t_p)$ from the equation $S_z(t) = 0$, $t = [t_0 = 0,\ t_1 \ldots t_n]$. Moreover, $\alpha_i(t_{p-1})$ can be deduced from differential equations Eq. (12), their components being assumed null at $t = 0$. For example, the component along z at $t = t_p$ can be estimated from its component at $t = t_{p-1}$ thanks to the equation:

$$\alpha_{zk}(t_p) = \frac{dt}{\lambda_k + dt}\left(-\frac{1}{3}E_x - \frac{1}{3}E_y + \frac{2}{3}E_z + \alpha_{zk}(t_{p-1})\right),\ 1 \le k \le N \tag{15}$$

The same kind of equation is solved to estimate $\alpha_{xk}(t_p)$ and $\alpha_{yk}(t_p)$, $\forall p \in [0 \ldots n]$.

At $t = t_p$, we can evaluate $S_x(t_p)$ et $S_y(t_p)$ thanks to Eq. (12).

These equations, implemented in MATLAB®, allow to depict the evolution of the internal residual stress (according to the direction x and y) taking into account the evolution of the behavior of material identify from previous shear tests (which allow the identification of G_0, G_∞ and for $k = 1 \ldots N$, τ_k, w_k) and according to the strain/temperature profiles measured through DIC/ infrared thermography (as boundary conditions). The nominal stress tensor is computed from the second Piola Kirchhof tensor *via* the relation: $\sigma = det(F)^{-1} FSF^t$ where F is the strain gradient.

6. Results and discussion

6.1. Boundary conditions

6.1.1. Rheological behavior of LDPE, LLDPE and their blends

In a first place, the sets of rheological parameters $\{G_k,\ \lambda_k\}$ given by (Eqs. (7) and (8) were identified based on a generalized Maxwell model associated with $N = 7$ elements for LDPE at 3 temperatures 150 °C, 170 °C, and 190 °C. The identification was performed by minimization (least-mean squares) between the numerical values of G', G'' and the corresponding experimental data obtained through oscillatory shear.

Loss and storage experimental moduli of LDPE were fitted by generalized Maxwell model as represented as an example in Fig. 4 and sets of $\{G_k,\ \lambda_k\}$ parameters are listed in Table 4. Smooth fits were obtained

Table 4
Identification of GMM parameters for LDPE at 150 °C, 170°C and 190°C.

#	T (°C)	150		170		190	
k	λ_k	G_k	w_k	G_k	w_k	G_k	w_k
0	0	$1.49.10^5$	–	$1.35.10^5$	–	$1.11.10^5$	–
1	10^{-4}	$2.3.10^{-4}$	$1.54.10^{-9}$	$2.3.10^{-4}$	$1.71.10-^9$	$2.3.10^{-4}$	$2.08.10^{-9}$
2	10^{-3}	$5.49.10^{-4}$	$3.6.10^{-9}$	$5.49.10^{-4}$	$4.07.10^{-9}$	$5.49.10^{-4}$	$4.97.10^{-9}$
3	10^{-2}	$9.39.10^4$	$6.3.10^{-1}$	$8.92.10^4$	$6.61.10^{-1}$	$7.64.10^4$	$6.91.10^{-1}$
4	10^{-1}	$3.52.10^4$	$2.4.10^{-1}$	$3.09.10^4$	$2.29.10^{-1}$	$2.43.10^4$	$2.20.10^{-1}$
5	1	$1.57.10^4$	$1.0.10^{-1}$	$1.21.10^4$	$8.95.10^{-2}$	$8.35.10^3$	$7.55.10^{-2}$
6	10^1	$4.05.10^3$	$2.7.\ 10^{-2}$	$2.50.10^3$	$1.86.10^{-2}$	$1.40.10^3$	$1.27.10^{-2}$
7	10^2	$5.72.10^2$	$3.8.10^{-3}$	$2.14.10^2$	$1.59.10^{-3}$	$7.93.10^1$	$7.18.10^{-4}$

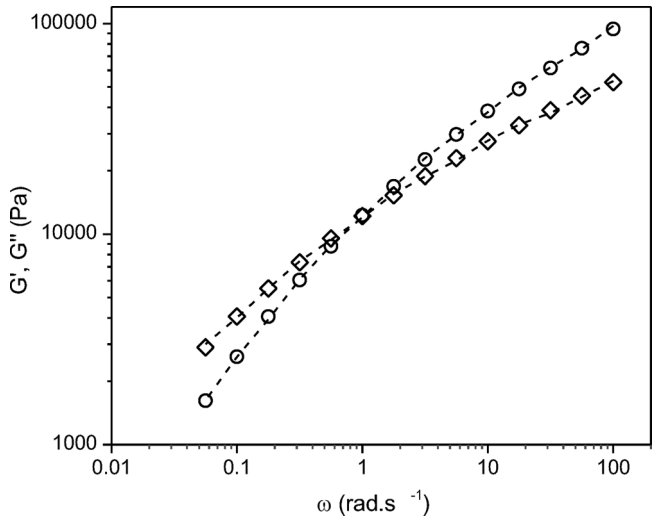

Fig. 4. Storage $G^{'}$(○) and loss $G^{''}$(◇) moduli experimental data fitted by the Generalized Maxwell Model (in dashed line) for the LDPE at 150 °C.

for all polymer blends.

This identification highlights the requirement to extrapolate the data of the generalized Maxwell model sets of parameters for the loading conditions undergone during the process. The behavior under small strain ($\gamma = 5\%$) is extrapolated to predict the behavior under larger strain and larger temperature scale experienced during the process.

As previously discussed, differences in molecular structures (long-chain/short-chain branching) may result in different rheological behaviors under the same solicitation and therefore in different moduli and relaxation times (*i.e.,* longer times are required for the LCB to relax compared to that of linear). Therefore, the sets of parameters of relaxation strength moduli and relaxation time $\{G_k, \lambda_k\}$ were implemented in the predictive model of the internal residual stress. In addition, these sets of rheological parameters were also dependent on the temperature profile over the stretching zone.

6.1.2. Photomechanical analysis

The strain profile (e_{L_M} as a function of e_{L_T}) of LDPE and LLDPE obtained for the two extreme values of take-up speeds (v_1 and v_6) through DIC are presented in Fig. 5. LDPE strain profile shows that the deformation takes place almost only along the machine direction while a substantial e_{L_T} strain is noticed in the case of LLDPE, whatever the take-up speed.

Furthermore, due to excessive velocity of the film, it is important to point out that the higher the take-up speed, the smallest is the distance that could be reached with the DIC. Insofar, for the highest speeds, the correlated distance from the die decreases and the extrapolation had to be done on a greater distance for high speeds than for low ones.

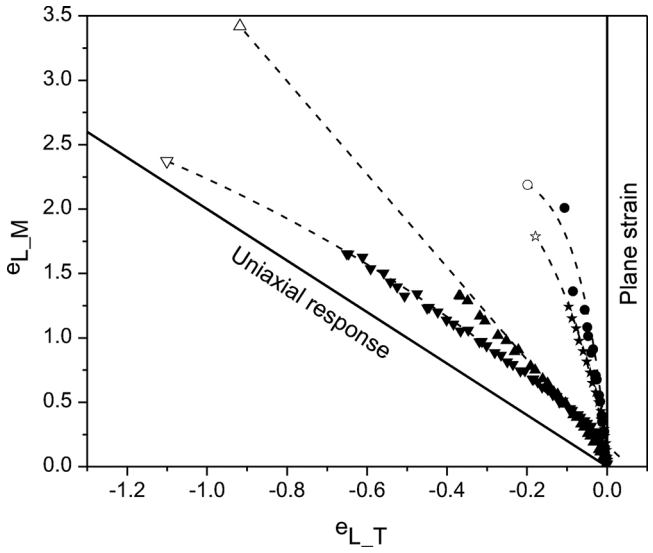

Fig. 5. Strain profiles at extreme draw ratio evaluated through DIC. For (★) LDPE at v_1 (●) LDPE at v_6 and (▼) LLDPE at v_1 (▲) LLDPE at v_6. Interpolation/extrapolation are represented in dashed lines. The corresponding open symbols represent the extrapolated value at $X = 135$ mm.

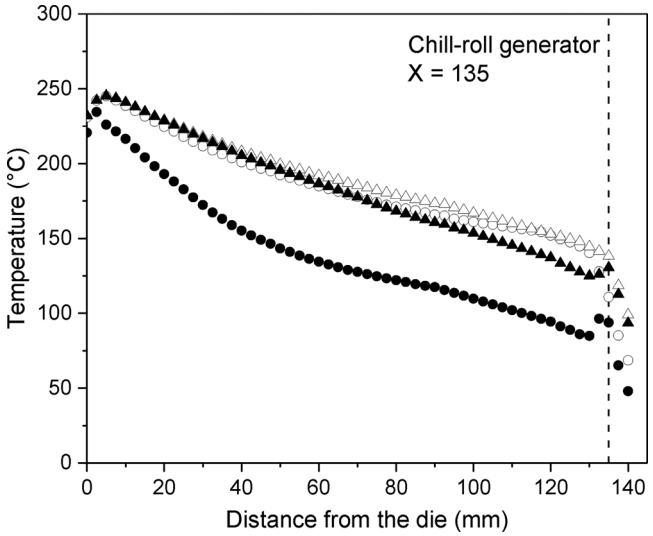

Fig. 6. Experimental Temperature profile of LDPE at v_1 (○) and v_6 (●) and of LLDPE at v_1 (△) and v_6 (▲).

Therefore, the extrapolation is more accurate for low take-up velocities than for higher ones.

6.1.3. Temperature profile

Fig. 6 presents the temperature profiles between the die and the chill rolls for LDPE and LLDPE for at the extreme values of DR (v_1 and v_6). The temperature at the die was set at 230 °C for all experiments. It should be pointed out that the temperature profiles of all polymers exhibit a shoulder at the die exit. The temperature on the stretching distance ranges from 245 °C to 85 °C when touching the roll. No major difference in the temperature profiles measured was noticed between v_1 and v_6 for the LLDPE whereas the temperature profile of LDPE at low take-up speed is similar to LLDPE ones but greatly differs at high take-up speed. Besides, the LDPE v_6 profile shows a higher cooling rate which could be attributed to the higher thickness reduction compared to the others.

These temperature profiles suggest that the polymer does not crystallize before it touches the chill rolls (T_c = 102°C) .

6.2. Simulated internal residual stress

From the knowledge of the boundary conditions that constitute rheological parameters, strain and temperature profile presented in Section 6.1, the internal residual stress stored during the stretching of the films was simulated according to the equations presented in Section 5. Numerical modeling.

The simulated internal residual stress stored in LDPE, LLDPE and 50/50% LDPE/LLDPE blends as a function of the time required to reach the roll generator (X = 135 mm) is represented in Fig. 7. Whatever the PE formulation and the take-up speed, it can be observed that the ultimate internal residual stress remains low below 4×10^5 Pa.

For LLDPE at v_1, the time at which the internal residual stress starts to increase almost exponentially is approximately 5 s whereas at v_6, this time is almost twice lower. For LDPE, the time at which the internal residual stress increases significantly is approximately 1 s whatever the take-up speed. The 50/50% LDPE/LLDPE blend exhibits an intermediate behavior. The stress deviates at 2.5 s at v_1 and at approximately 1.5 s at v_6. At the lowest take-up speed v_1, the internal residual stress appears to grow sharply at lower times, this phenomenon being more pronounced for higher amount of LDPE. From these findings, it can be proposed that LCB contained in LDPE result in higher entanglements which promote an earlier storage of the internal residual stress compared to the linear structure of LLDPE. Moreover, the behavior of the

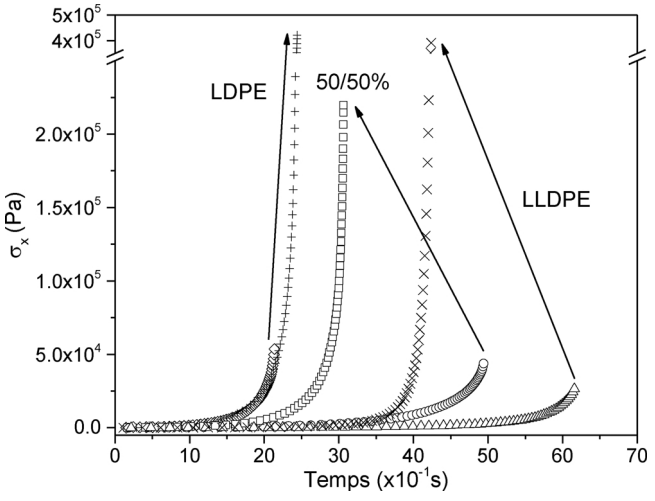

Fig. 7. Simulated internal residual stress profile of LDPE at v_1 (◇) and v_6 (+), 50/50% LDPE/LLDPE at v_1 (○) and v_6 (□), and LLDPE at v_1 (△) and v_6 (×) *versus* time.

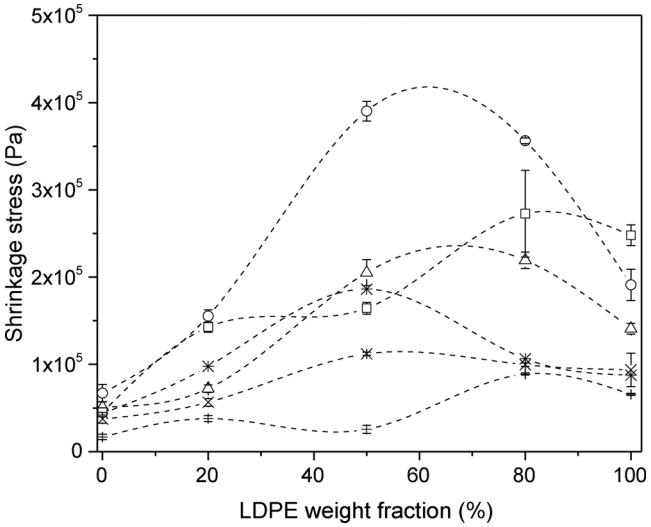

Fig. 8. Experimental shrinkage (residual stress) *versus* LDPE weight fraction for v_1 (+), v_2 (×), v_3 (✳), v_4 (△), v_5 (□), and v_6 (○).

blends seems to indicate that the time required to store a defined level of stress during the stretching is related to the LCB content, *i.e.* the amount of LDPE in the blend is well correlated to the time required to store a defined level of stress during the stretching. Furthermore, increasing the take-up speed leads to similar effect than increasing LCB content, an earlier and more pronounced increase of the internal residual stress stored in the polymer melt. As a matter of fact, it was shown that LCB content was well related to the characteristic relaxation times of the chains and that LLDPE always exhibited lower relaxation times than LDPE rich-blends. Therefore, it can be suggested that increasing the speed prevents the chains from relaxing in the time of the stretching stage.

7. Comparison between simulated internal residual stress and measured shrinkage stress

Restrained shrinkage experiments in DMTA were carried out on all films and for all take-up speeds. When the sample was immersed in the oil bath maintained at 130 °C, a shrinkage force, corresponding to the relaxation of the films frozen in a stretched state at the end of the film extrusion process, can be recorded. When the films were totally relaxed, the recorded force suddenly drops down and the sample was manually pulled off the oil bath. Therefore, the force spectrum exhibits a peak which is defined as the shrinkage force. Fig. 8 presents the experimental restrained shrinkage stress *versus* the LDPE weight fraction.

It should be emphasized that all the internal residual stress accumulated during the stretching process is expected to be released instantaneously during the shrinkage experiments. Indeed, the quenching at 130 °C is sufficiently fast to allow the stress to be quasi-instantaneously released, *i.e.*, preventing the polymer chains to relax and rearrange slowly which would compensate the sudden stress release by a slow conformational change recovering the deformation.

Whatever the take-up speed considered, the LDPE always exhibits a higher shrinkage stress than LLDPE. LLDPE shrinkage stress at v_1 (1.69×10^4 Pa) is approximately four times lower than those at v_6 (6.71×10^4 Pa) but the values remain low compared to those recorded for LDPE. Indeed, the shrinkage stress of LDPE increases from 6.56×10^4 Pa at v_1 to 1.91×10^5 Pa at v_6. Even though the 20/80 LDPE/LLDPE blend exhibits shrinkage stress values that increased according to the take-up speed, this observation is not confirmed for the other blends and for LDPE. Moreover, no final conclusion can be drawn from the behavior of the pure matrices and the LDPE/LLDPE blends at a given take-up speed. Shrinkage stress seems though to highlight a

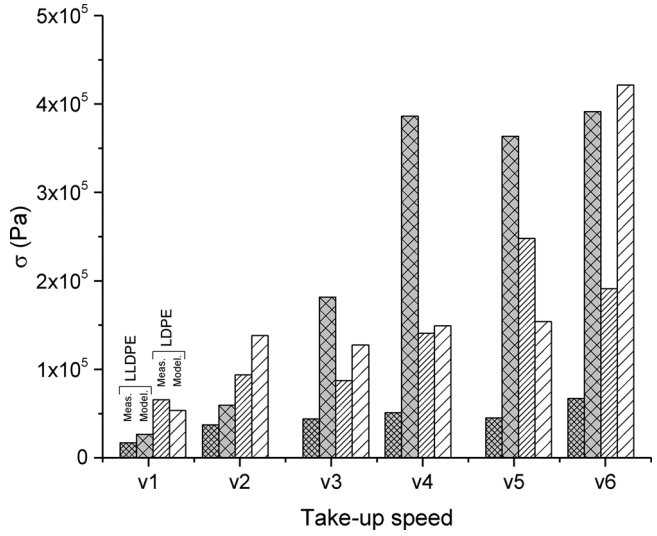

Fig. 9. Comparison between simulated stress and experimental stress measured by DMTA as a function of take-up speed v_x of LDPE and LLDPE.

synergistic effect for the blends, but this synergistic effect does not follow any particular law, being sometimes negative or positive and seems to be shifted on blend compositions for the various take-up speeds. The largest discrepancies in shrinkage stress according to the take-up speeds is found for the 50/50% LDPE/LLDPE blend which increases by more than a decade from v_1 to v_6.

The simulated data of the internal residual stress are compared to those of the restrained shrinkage stress obtained by DMTA experiments (Fig. 9) for LDPE and LLDPE.

The simulated internal residual stress and experimental restrained shrinkage stress exhibit values in the same order of magnitude although the simulated values are systematically higher than the measured ones. Moreover, larger discrepancies are found for take-up speeds larger than v_3, especially for LLDPE. Interestingly, LDPE simulated internal residual stress and shrinkage stress are close, even for high take-up speeds, even though the model deviates strongly above the take-up speed v_5.

Several hypotheses could explain the deviations of the modeled residual stress compared to those of experimental restrained shrinkage. As mentioned above, the higher the take-up speed (velocity), the greater distance extrapolated is needed to depict the strain between the die and the roll. Also, even though the process involves large deformations, we choose a model for small deformations, in the linear viscoelastic domain.

The generalized Maxwell model was fitted on rheological data obtained from shear tests in the linear viscoelastic domain (at $\gamma = 5\%$) and extrapolated at higher deformations and larger temperature scale undergone by the melt during the stretching. Indeed, the highest value predicted from DIC $E_{L\_M} = 3.43$ obtained for the LLDPE at v_6 correspond to a dilatation of 3000% which is out of the linear viscoelastic domain.

Finally, even though deviation have been found, it is worth mentioning that measured internal residual stress and simulated one are in the same order of magnitude which constitute an encouraging result.

8. Conclusion

The internal residual stress stored within the polymer film during the stretching phase of the cast film extrusion process has been modeled. First, a generalized Maxwell model with 7 elements was fitted on the storage and loss moduli data (for all LDPE/LLDPE compositions and for all temperatures) obtained through oscillatory shear tests. The resulting boundary conditions used sets of parameters $\{G_k, \lambda_k\}$, as associated with the temperature and strain profiles allowed to predict the biaxial stress undergone during the stretching process. The modeled ultimate stress stored in LDPE and LLDPE films was compared to the shrinkage stress measured by DMTA. Both stresses were found to be in the same order of magnitude.

Besides, the branched and linear materials revealed significant differences in their behavior. The global deformation response under the large elongation undergone during the stretching was found to be definitely biaxial for the LDPE whereas the LLDPE response was quasi-uniaxial. This is an interesting result considering that LDPE and LLDPE were processed under the same operating conditions. These contrasted responses of the films under stretch have been justified by differences in their rheological behavior, primarily due to the presence of LCB in LDPE.

From the temperature profile, the generalized Maxwell model parameters were interpolated in the range of temperatures performed in the rheological tests and extrapolated out of this range. Moreover, the photomechanical analysis and digital image correlation were carried out to establish planar strain profiles. Smooth strain profiles were obtained at low velocities but the need of an extrapolation on a greater distance as the take-up speed increased was highlighted. This could constitute one possible reason explaining the deviation between modeled and experimental data of shrinkage stress. The strain profiles at high take-up speed may be obtained over the entire distance without any extrapolation required if using a high-speed camera.

The generalized Maxwell model is often used to describe viscoelastic (*i.e.*, small deformations) polymeric melts. However, the non-linear behavior of the material during the cast film process requires extrapolations that may also constitute a valid reason for the deviation observed between the modeled internal residual stress and the shrinkage stress.

Numerical simulation constitutive equations were established corresponding to biaxial deformations.

Finally, the stress storage rate is such as the sensitivity of the time increment on the numerical value would require a deeper analysis.

Further work will consist in integrating non-linear rheological behavior of the matrix that could predict closely the reality of the blowing process. This is particularly true for LCB polymers that exhibit high strain hardening at high deformation rate like those encountered in the blowing process.

This work was a part of a Ph.D. aiming at substituting an oil-based matrix by a biodegradable biopolyester to demonstrate its potential use in heat-shrinkable film for packaging application. Therefore, the model could be applied to predict the residual stress of a potential new matrix of different architecture (*e.g.* crosslinked) to know if it would be suitable for this specific application.

Acknowledgments

Authors are embedded to the French Environment and Energy Management Agency-ADEME (no TEZ11-26) and to Ceisa Packaging Company (Bernay, France) for their financial support.

References

Agassant, J.F., Demay, Y., Sollogoub, C., Silagy, D., 2005. Cast film extrusion. Int. Polym. Process. 20, 136–148. https://doi.org/10.3139/217.1874.

Barot, G., Rao, I.J., 2005. Modeling the film casting process using a continuum model for crystallization in polymers. Int. J. Non-Linear Mech. 40, 939–955. https://doi.org/10.1016/j.ijnonlinmec.2004.07.012.

Barq, P., Haudin, J.M., Agassant, J.F., 1992. Isothermal and anisothermal models for cast film extrusion. Int. Polym. Process. VII, 271–283.

Boulahia, R., Boukharouba, T., Glaoguen, J.M., 2013. The Use of the DIC Method to Involve the Strain Instability Occurred in an Undergoing High Shear During the ECAE Process. Springer, Berlin, Heidelberg, pp. 567–574. https://doi.org/10.1007/978-3-642-37143-1_68.

Caro-Bretelle, A.S., Ienny, P., Nait-Ali, L.K., Bergeret, A., 2013. Dissipative behaviour analysis of beprocessed polyethylene terephthalate using digital image correlation and updated finite element analysis. Strain 49, 135–146. https://doi.org/10.1111/str.12021.

Cotto, D., Duffo, P., Haudin, J.M., 1989. Cast film extrusion of polypropylene films. Int. Polym. Process. IV, 103–113.
Demay, Y., Agassant, J.-F., 1996. An overview of molten polymer drawing instabilities. Int. Polym. Proc. 1–24.
Ferry, J.D., 1980. Viscoelastic Properties of Polymers. John Wiley & Sons, New York.
Green, A.E., Rivlin, R.S., 1957. The mechanics of non-linear materials with memory. Arch. Ration. Mech. Anal. 1, 1–21. https://doi.org/10.1007/BF00281398.
Haudin, J.M., Piana, A., Monasse, B., Gourdon, B., 2003. Étude des relations entre mise en forme, orientation et rétraction dans des films de polyéthylène basse densité réalisés par soufflage de gaine IV. Étude de la rétractionhaudin. Ann. Chim. Sci. des Mater. 28, 91–107. https://doi.org/10.1016/S0151-9107(03)00009-6.
Jay, F., Monasse, B., Haudin, J.M., 1998. Memory effects in crystallization of polypropylene during cast film extrusion. Int. J. Form. Process. 1, 75–95.
Keller, A., Machin, M.J., 1967. Oriented crystallization in polymers. J. Macromol. Sci. Part B Phys. 1, 41–91.
Lamberti, G., Titomanlio, G., Brucato, V., 2002. Measurement and modelling of the film casting process. 1. Width distribution along draw direction. Chem. Eng. Sci. 57, 1993–1996. https://doi.org/10.1016/S0009-2509(02)00098-2.
Laraba-Abbes, F., Ienny, P., Piques, R., 2003a. A new 'Tailor-made' methodology for the mechanical behaviour analysis of rubber-like materials: II. Application to the hyperelastic behaviour characterization of a carbon-black filled natural rubber vulcanizate. Polymer 44, 821–840. https://doi.org/10.1016/S0032-3861(02)00719-X.
Laraba-Abbes, F., Ienny, P., Piques, R., 2003b. A new 'tailor-made' methodology for the mechanical behaviour analysis of rubber-like materials: I. Kinematics measurements using a digital speckle extensometry. Polymer 44, 807–820. https://doi.org/10.1016/S0032-3861(02)00718-8.
McNally, G.M., 2005. J. Plast. Film Sheeting 21, 39–54. https://doi.org/10.1177/8756087905052804.
Muniandy, K., Ariff, Z.M., Bakar, A.A., 2018. Online strain measurement during blown film extrusion. J. Mech. Eng. 5, 154–165.
Pearson, J.R.A., 1966. Mechanical Principle of Polymer Melt Processing. Pergamon Press, Oxford.
Sergent, J.-P., 1977. Etude de deux procédés de fabrication de films. Le soufflage de gaine. L'extrusion de film à plat.
Ward, I.M., 1997. Structure and Properties of Oriented Polymers, 2nd ed. Springer.